Light/dark and temperature cycling modulate metabolic electron flow in *Pseudomonas aeruginosa* biofilms

Lisa Juliane Kahl[a], Kelly N. Eckartt[a], Diana K. Morales[a]*, Alexa Price-Whelan[a], Lars E. P. Dietrich[a]#

[a]Department of Biological Sciences, Columbia University, New York, NY, USA

Running title: Light and temperature cycling alter biofilm metabolism

Word count (abstract; impact; main text): 4821

#Address correspondence to Lars Dietrich, ldietrich@columbia.edu

*Present address: Lisa Juliane Kahl, Charité Universitätsmedizin Berlin, Institute of Biochemistry, Berlin, Germany; Diana K. Morales, Department of Obstetrics and Gynecology, Weill Cornell Medical College, New York, NY, USA

Lisa Juliane Kahl and Kelly N. Eckartt contributed equally to this work. Author order was determined on the basis of seniority.

ABSTRACT (250 word limit)

Sunlight drives phototrophic metabolism, which affects redox conditions and produces substrates for non-phototrophs. These environmental parameters fluctuate daily due to Earth's rotation, and non-phototrophic organisms can therefore benefit from the ability to respond to, or even anticipate, such changes. Circadian rhythms, such as diurnal changes in body temperature, in host organisms can also affect local conditions for colonizing bacteria. Here, we investigated the effects of light/dark and temperature cycling on biofilms of the opportunistic pathogen *Pseudomonas aeruginosa* PA14. We grew biofilms in the presence of a respiratory indicator dye and found that greater dye reduction occurred in biofilm zones that formed during dark intervals and at lower temperatures. This pattern formation occurred with cycling of blue, red, or far-red light, and a screen of mutants representing potential sensory proteins identified two with defects in pattern formation specifically under red light cycling. We also found that the physiological states of biofilm subzones formed under specific light and temperature conditions were retained during subsequent condition cycling. Light/dark and temperature cycling affected expression of genes involved in primary metabolic pathways and redox homeostasis, including those encoding electron transport chain components. Consistent with this, we found that cbb_3-type oxidases contribute to dye reduction under light/dark cycling conditions. Together, our results indicate that cyclic changes in light exposure and temperature have lasting effects on redox metabolism in biofilms formed by a non-phototrophic, pathogenic bacterium.

IMPORTANCE (150 word limit)

Organisms that do not obtain energy from light can nevertheless be affected by diurnal changes in light exposure. Many aspects of animal and fungal physiology fluctuate in response to these changes, including body temperature and the activities of antioxidant and other redox enzymes that play roles in metabolism. Whether redox metabolism is affected by light/dark and temperature cycling in bacteria that colonize such circadian organisms has not been studied in detail. Here we show that growth under light/dark and temperature cycling leads to rhythmic changes in redox metabolism in *Pseudomonas aeruginosa* and identify proteins involved in this response. *P. aeruginosa* is a major cause of healthcare-associated infections and designated as a serious threat by the CDC due to its recalcitrance during treatments. Our findings have the potential to inform therapeutic strategies that incorporate controlled light exposure or consider *P. aeruginosa*'s responses to conditions in the host.

INTRODUCTION

Sunlight powers most biology and, via its role in phototrophic metabolism, influences cellular and environmental redox potentials. Oxygenic phototrophs in particular, which are thought to have evolved over 2.4 billion years ago (1), use light to produce a strong oxidant (oxygen) that affects external conditions. Light and redox therefore have a long-standing relationship in Earth's history, and because light is only available for a limited portion of each day, redox conditions fluctuate with corresponding regularity (2–5). Though non-phototrophic (i.e., chemotrophic) bacteria do not depend on light as an energy source, they nevertheless can be directly affected, for example, by the impact of light on cellular cofactors, or indirectly affected by the impact of light on the environment. Commensal and pathogenic bacteria can also indirectly experience the effects of light via host circadian rhythms, such as diurnal fluctuations in body temperature (6–9).

Studies examining (i) responses to visible light exposure or (ii) endogenous physiological rhythms that are entrained by light cues have revealed linkages between redox physiology and light in chemotrophs. In many chemotrophs, substrates donate electrons to central metabolic pathways, which rely on redox reactions to ultimately produce a membrane potential that drives ATP synthesis. Visible light has been shown to affect central metabolism and/or membrane potential in chemotrophic flavobacteria, *Escherichia coli*, *Bacillus subtilis*, and budding yeast (10–13). For diverse organisms that exhibit light-entrainable and endogenous physiological rhythms, it has been shown that these rhythms correlate with changes in the redox states of antioxidant/signaling proteins called peroxiredoxins (14). Budding yeast also shows endogenous respiratory oscillations that bear similarities to light-entrainable, endogenous physiological rhythms in other organisms (15), which may hint at an ancestral relationship between redox state and cyclic changes in light exposure. Together, these findings point to fundamental influences of Earth's fluctuating light conditions on cellular electron-transfer metabolism.

In this study, we investigated the effects of light/dark and temperature cycling on redox biology in *Pseudomonas aeruginosa*, a major cause of biofilm-based infections. Our results indicate that cycling these stimuli leads to oscillations in routes of metabolic electron flow that are mediated by global changes in transcription. They also suggest that *P. aeruginosa*'s terminal oxidases contribute to the changes in respiratory activity that occur during biofilm growth under light/dark cycling conditions. These findings highlight the strong potential influence of fluctuating environmental and host conditions during infection, and the importance of considering these factors when designing treatment approaches.

RESULTS

Growth with constant light exposure affects TTC reduction activity in Pseudomonas aeruginosa *PA14 biofilms*

The formation of *P. aeruginosa* biofilms, which is dependent on the extent and timing of biofilm matrix production, is highly sensitive to the availability of respiratory substrates and the capacity for aerobic and anaerobic metabolisms (16, 17). Recently, we showed that *P. aeruginosa* biofilm development is also affected by light exposure and that interestingly, one of the proteins that regulates this process appears to integrate light and redox information (18). These observations raised the question of whether light exposure affects redox metabolism in *P. aeruginosa*. To test this, we adapted an assay based on reduction of the redox indicator triphenyl tetrazolium chloride (TTC) (19–22). TTC is colorless in its oxidized form; it is reduced by components of the electron transport chain and subsequently forms a red precipitate (**Figure 1A, Figure S1**). We added TTC to agar-solidified media for the growth of colony biofilms of *P. aeruginosa* PA14 (**Figure 1B**). For these experiments, we used a PA14 Δ*phz* mutant because this strain is unable to produce phenazines, endogenous redox-cycling compounds that have the potential to react with tetrazolium salts and therefore could interfere with the TTC assay (23).

We grew biofilms on TTC-containing media and compared those grown in darkness to those grown with constant exposure to white light, at an intensity comparable to sunlight on a winter day in the Northern Hemisphere (100 µmol photons m^{-2} s^{-1}) (24). We found that growth with constant light led to lower levels of TTC reduction overall than growth in darkness (**Figure 1C, D**). Biofilms grown in either condition also showed overall decreases in the amount of TTC reduction as they grew, with the biofilm center (older growth) showing more TTC reduction than the biofilm edge (younger growth).

Light/dark and temperature cycling elicits bands of entrenched TTC reduction activity in PA14 biofilms

On much of Earth's surface, sunlight exposure occurs for a limited time interval each day. We therefore asked how periodic exposure to light would affect TTC reduction by growing biofilms under conditions of light/dark cycling. After inoculation, biofilms were subjected to 12 hours of white light, followed by 12 hours of darkness, and this 24-hour cycle was repeated 5 times for a total of 6 days of growth. We expected these conditions to yield intermediate levels of TTC reduction throughout the biofilm, comparable to the average of that observed for constant dark and constant light conditions. However, we instead found that biofilms grown with light/dark cycling showed rings of differential TTC reduction that were not present in biofilms grown under constant conditions (**Figure 1E**).

Diurnal changes in light exposure can be accompanied by changes in temperature, for example when bacteria colonize a host exhibiting circadian rhythms in body temperature, which typically varies by 2˚ to 3˚C (8). To test whether small changes in temperature affect TTC reduction, we grew biofilms with temperature cycling (ΔT = 2˚C in constant dark or constant light) and found that this condition also yielded characteristic bands of TTC reduction in biofilms (**Figure 1F, Figure S2**). Combining both light and temperature cycling (i.e., repeating intervals of 12 hours of white light at 25˚C followed by 12 hours of darkness at 23˚C) gave rise to the most well-defined TTC ring phenotype (**Figure 1G**), and we therefore used these conditions for additional experiments in biofilms. First, we tested whether the TTC reduction pattern is determined by the duration of intervals during light/dark and temperature cycling, by growing biofilms under shortened (conditions alternating every 6 h) or lengthened (conditions alternating every 24 h) intervals. We found that bands of TTC reduction correlated with the altered intervals (**Figure 2**).

Next, and to better understand the dynamics of TTC reduction, we built a custom-made set up that allowed us to capture images of growing biofilms every 30 minutes (**Figure S3**). Using these images, we generated kymographs that visualize temporal changes in TTC reduction for pixels appearing at successive time points at the leading edge of the biofilm, along a selected radius (**Figure 3A**). These kymographs show an increase in red color over time for biomass that became visible under either dark or light conditions. However, they also show that biomass that first became visible under dark conditions reduced more TTC overall than prior growth that first became visible under light conditions, thereby yielding the banding pattern. We then quantified these changes in pixel intensity by averaging the intensity for pixels at a given circumference of the biofilm and tracking how intensity increased over time for this ring of biomass (**Figure 3B**). This analysis revealed discrete metabolic subzones that formed as the biofilm grew outward: Rings that formed in the dark showed, overall, larger increases in TTC reduction over the course of the experiment than rings that formed in the light (**Figure 3B**). Notably, the intensities of pixels that originated in a specific dark period approached similar values (“clustered”) (**Figure 3B, top right**), while those that originated in a specific light period showed a broader range of values due to a stronger attenuation in final intensities for pixels that appeared later in the period (**Figure 3B, bottom right**). Differences in the kinetics of TTC reduction were particularly noticeable after the initial phase of rapid reduction that occurred in all subzones (**Figure 3B**).

Because an entire biofilm is exposed to cycling conditions, the observed TTC reduction patterns suggest that conditions present during the initial formation of a specific ring of growth serve to “set” the metabolic status of that zone for the remainder of the experiment (**Figure 4A**). To further test whether metabolic states that arise during cycling are maintained in mature biofilms, we repeated the

experiment but only exposed the biofilms to TTC after they had experienced the cycling regime. Specifically,e grew colony biofilms under light/dark and temperature cycling conditions for 144 hours on a medium without TTC, then transferred them to a medium containing the redox dye and incubated them for 270 minutes in darkness at 23˚C. Indeed, these biofilms formed distinct rings of TTC reduction, particularly visible closer to the biofilm edge (**Figure 4B**), indicating that metabolic status becomes entrenched during initial biofilm zone formation and is then maintained for hours to days.

The effect of light/dark cycling on TTC reduction is observed at different wavelengths of light and involves wavelength-specific sensory proteins

While white light comprises a range of wavelengths from ~400-700 nm, physiological responses to light are typically specific to a narrower range of wavelengths due to the unique sensitivities of protein cofactors or small molecules. To test if specific wavelengths are responsible for the effects of light/dark cycling on TTC reduction in biofilms, we grew biofilms under cycling with blue, red, or far-red light while keeping the temperature constant at 25˚C. We found that all three conditions yielded rings of TTC reduction like those observed under cycling with white light, indicating that light/dark cycling with different wavelengths of light can affect respiratory electron transport (**Figure 5**).

We next asked if PA14 has dedicated sensors that regulate TTC reduction during exposure to each range of wavelengths. Light-sensing proteins have been found in diverse eukaryotes, archaea, and bacteria, including many non-phototrophs (25–29). These proteins contain light-sensitive domains linked to regulatory domains that (i) themselves control intracellular signaling or gene expression, or (ii) interact with other proteins that perform these functions (29–31). Though the PA14 genome harbors only one gene encoding a canonical light-sensing domain--for the bacteriophytochrome BphP--it also contains genes for dozens of other proteins with PAS or GAF domains, which are broadly implicated in responses to light. These include the protein RmcA, which contains 4 PAS domains and which mediates an effect of constant light exposure on PA14 biofilm morphogenesis (18). We obtained mutants lacking each of the PAS- and/or GAF-domain-containing proteins and screened for effects on the characteristic TTC reduction pattern that we observe for the parent strain under light/dark cycling with blue, red, or far-red light. We found that mutants with disruptions in either *bphP* or *ptsP* showed little to no TTC reduction patterning under red light/dark cycling but retained the ability to produce the TTC reduction pattern under blue or far-red light/dark cycling (**Figure 5**). The results of our screen suggest that BphP and PtsP contribute to the effects of red light on TTC reduction in *P. aeruginosa* biofilms. We did not identify candidate blue-light or far-red light sensors in the screen; for blue light, this could be because there are multiple proteins that mediate the effects of blue light on TTC reduction or because blue light has pleiotropic effects (12, 32–35). We were surprised to find that the *bphP* mutant

did not show altered TTC reduction when grown under cycling blue or far-red light because recent work has indicated that BphP is activated by these (in addition to red light) (29).

Light/dark and temperature cycling yields zones of biofilm growth that are transcriptionally entrenched

As described above, the patterns in biofilms grown under light/dark cycling suggest that the conditions present during the initial formation of a ring of growth serve to determine the metabolic status of that ring for the remainder of the experiment, even though conditions continue to cycle throughout (**Figure 4A**). We hypothesized that these entrenched physiological states would be detectable at the level of gene expression. To test this, we used laser capture microdissection microscopy to sample from four adjacent zones of duplicate biofilms, i.e., two zones formed during light intervals and two zones formed during dark intervals for each of two biofilms and performed RNA sequencing analysis (RNAseq) (**Figure 6A, top**). Principal component analysis confirmed for all but one sample that initial exposure to light or dark resulted in and contributed the most to differential transcriptomic profiles (**Figure S4**). The outlier sample was excluded from further analysis. We found that although transcriptomes were assessed at a final time point and the entire biofilm had been exposed to light/dark cycling conditions for days, differences in expression were maintained (**Figure 6A bottom, B**). This confirms that, as suggested above by our observations of respiratory activity (**Figures 1-3 and 4B**), cells become "physiologically imprinted" by the conditions under which their zone of the biofilm forms. In other words, cells that are situated at the leading edge of the biofilm under dark conditions become strong TTC reducers and express a distinct set of genes from cells that are situated at the leading edge under light conditions, which become weak TTC reducers. Using a 2-fold change cutoff, we found that 341 genes were upregulated in biofilm zones that formed during light exposure and that 170 genes were upregulated in zones formed during dark intervals (**Figure 6B; Supplemental file 1**).

Upon examining the identities of genes affected by light/dark cycling, we noticed a strong representation of those involved in central metabolism, respiration, and redox homeostasis--consistent with the effects of light/dark cycling on TTC reduction. In particular, the KEGG-defined pathways of the pentose phosphate pathway, oxidative phosphorylation, glutathione metabolism, and purine metabolism (36) showed substantial representation of genes that were differentially expressed during light/dark cycling (**Figure 6C**). For each of these pathways, the genes that were differentially expressed were not consistently associated with biofilm zone formation during either light or dark intervals; rather, each pathway contained distinct subsets of genes that were upregulated in zones formed in either the light or the dark. For some pathways, these subsets of genes were linked by common features or functions. In the pentose phosphate pathway, for example, genes involved in the oxidative branch were upregulated in zones formed during light intervals, and genes involved in the non-oxidative branch were

upregulated in zones formed during dark intervals (**Figure S5**). For oxidative phosphorylation, we saw two distinct groups of genes for terminal oxidase components that clustered with respect to their expression profiles (**Figure 7A, B**). Genes coding for components of the cyanide-insensitive oxidase ("Cio"), the *bo*$_3$ terminal oxidase ("Cyo"), and the *aa*$_3$ terminal oxidase ("Cox") form the first group and were downregulated in rings of growth that formed during dark intervals and upregulated in those that formed during light intervals (**Figure 7A**). In contrast, genes coding for components of *cbb*$_3$-type cytochrome *c* oxidase complex CcoN1O1Q1P1 ("Cco1") and for the orphan terminal oxidase proteins CcoN4Q4, which form the second group, were downregulated in rings of growth that formed during light intervals and upregulated in those that formed during dark intervals (i.e., the opposite expression profile of the first group) (**Figure 7A**). The expression profiles of terminal oxidase genes observed under light/dark and temperature cycling in biofilms suggest that the preferential use of terminal oxidases shifts during cycling. We were intrigued to see that the set of terminal oxidase genes showing the largest change in expression during light/dark and temperature cycling was the *cyoABCDE* operon, because this locus is not expressed at high levels in typical aerobic or microaerobic planktonic cultures grown in the laboratory (37). Overall, the effects of light/dark cycling on gene expression in PA14 biofilms are consistent with observations of diurnal changes in light exposure affecting central metabolism, respiration, and redox homeostasis in other organisms (14, 38–40).

cbb$_3$*-type terminal oxidases contribute to TTC reduction in rings formed during dark intervals*

Components of *cbb*$_3$-type terminal oxidases are encoded by 4 different loci in the PA14 genome. Two of these gene clusters, *ccoN1O1Q1P1* (*cco1*) and *ccoN2O2Q2P2* (*cco2*), are each sufficient to produce a complete functional oxidase, i.e., they contain all of the components of a *cbb*$_3$-type complex. Two others, *ccoN3Q3* and *ccoN4Q4*, are "orphan" clusters that each contain two subunits that can substitute for subunits encoded by the 4-gene operons. Genetic and biochemical analyses have shown that *cbb*$_3$-type oxidase isomers containing almost all combinations of subunits from each of these loci are functionally similar (41), though the differential expression of *cco* gene loci can affect their relative contributions under specific growth conditions (17, 37). In our RNAseq analysis, we observed that *cco1* and *ccoN4Q4* showed a similar pattern of relatively high expression in biofilm zones that formed during dark intervals and relatively low expression in biofilm zones that formed during light intervals. We therefore hypothesized that *cbb*$_3$-type terminal oxidases contribute to TTC reduction in rings formed during dark intervals. Because *P. aeruginosa* possesses multiple terminal oxidases that could function in a compensatory manner (42), we were unsure whether a *cbb*$_3$-type terminal oxidase mutant would show a detectable phenotype for TTC reduction. Nevertheless, we grew (i) a Δ*phz*Δ*cco1cco2* mutant, which is unable to produce functional *cbb*$_3$-type terminal oxidases and (ii) Δ*phz* PaCco1, which contains Cco1 and the two orphan clusters CcoN3Q3 and CcoN4Q4, but lacks Cio, Cox, Cyo and Cco2, and

compared these to the Δ*phz* parent strain on solidified media containing TTC with light/dark and temperature cycling. We then analyzed the increase in pixel intensity over time for each zone of the biofilm as described above for **Figure 3.** TTC reduction curves for biomass that formed in the first 60 hours of growth are shown in **Figure 7C**, and images of corresponding biofilms are shown in **Figure S6**. Similar final TTC reduction values were observed for the biomass formed by Δ*phz*, Δ*phz*Δ*cco1cco2*, and Δ*phz* PaCco1 in the first 60 hours of growth. The Δ*phz* PaCco1 strain and the parent strain also showed similar TTC reduction dynamics, indicating that Cco1 is sufficient to support wild-type patterns of respiration in light/dark cycling conditions. By contrast, the Δ*phz*Δ*cco1cco2* mutant showed altered TTC reduction dynamics, with rates of reduction that were lower than those of the parent strain for most of the incubation (**Figure 7D**). Comparing the Δ*phz*Δ*cco1cco2* mutant to the parent strain, we observed that the increase in TTC reduction rate was more gradual and that maximum rates of reduction tended to occur ~10-20 hours later, i.e., roughly one interval later, for the mutant lacking cbb_3-type oxidases.

DISCUSSION

Though chemotrophic bacteria do not depend on light as an energy source, they are impacted by light exposure, or fluctuations in light exposure, in several ways. Light affects environmental conditions by driving the metabolisms of phototrophs, which produce oxidants and other resources that can be used by chemotrophs (43–45). Light can also directly damage cofactors required for chemotrophic metabolisms (12, 32–35). Finally, light affects the physiologies of circadian organisms that act as hosts for commensal or pathogenic bacteria and thereby leads to diurnal oscillations in parameters such as temperature (8).

We investigated whether growth under light/dark and temperature cycling affected metabolism and gene expression in colony biofilms of *P. aeruginosa* PA14, a chemotrophic bacterium and opportunistic pathogen. We found that growth of PA14 biofilms under either light/dark or temperature cycling promoted the formation of rings of alternating levels of metabolic activity, as indicated by reduction of the dye TTC. When biofilms were grown under conditions of alternating intervals of dark at 23 °C and light at 25 °C, the formation of rings with increased activity correlated with growth under dark and low-temperature conditions and adjusted to the period length. We also found that cycling of blue, red, and far-red light were each sufficient to elicit ring formation. RNAseq analysis of samples taken from rings of high or low TTC reduction activity revealed differences in the expression of genes involved in primary metabolism and redox homeostasis. Our results suggest that the conditions that prevail during growth of a specific zone of the biofilm serve to “set” the physiological status of that zone, because although entire biofilms were exposed to cycling conditions, individual zones of these biofilms showed differences in TTC reduction activity and gene expression. Consistent with this, we also observed that

the formation of bands of TTC reduction in biofilms that were grown under cycling conditions on a medium without the dye and subsequently transferred to a medium containing the dye.

Ring or band patterning has been described for biofilms formed by various chemotrophic bacteria and fungi. Perhaps the most well-known of these is the model microbial fungus *Neurospora crassa*, in which conidiation is used as a readout for the circadian rhythm because it occurs diurnally under specific redox conditions (46). *N. crassa* rhythmic biology has been shown to conform to the definition of a circadian phenomenon and the biochemical basis of circadian regulation in this organism is well understood. Recently, colony biofilms of the soil and human gut commensal bacterium *B. subtilis* were shown to exhibit rings of gene expression that form autonomously (47). Circadian changes in gene expression and fluctuations in cellular differentiation have also been associated with biofilm formation in this organism (48). Other microbes that have been shown to form ring or band patterns that exhibit rhythmicity include *P. putida*, *L. monocytogenes*, *K. aerogenes,* and dimorphic and cold-adapted yeast (49–53). While some of these phenotypes require growth under light/dark or temperature cycling conditions, others occur autonomously.

We observed that light/dark cycling during growth of *P. aeruginosa* biofilms affected respiratory activity and redox metabolism. Control of primary metabolism and redox homeostasis in response to light/dark cycling or as part of a biological oscillation has been reported for diverse phototrophs (as would be expected for organisms that use light as an energy source; (54–56)) and non-phototrophs (38, 57, 58). A comprehensive study of organisms representing all domains of life showed circadian oscillations between the oxidized and superoxidized states of peroxiredoxins, broadly conserved enzymes that control intracellular levels of reactive peroxides and that can serve as indicators of redox homeostasis. These results suggest that circadian rhythms evolved in association with diurnal changes in cellular redox metabolism (14). The budding yeast *Saccharomyces cerevisiae* does not exhibit circadian rhythms, but rather an ultradian phenomenon referred to as yeast metabolic cycling or respiratory oscillation. This can be observed as ultradian O_2 fluctuations in continuous cultures and arises spontaneously, specifically in cultures that are at high density and nutrient limited. Numerous studies have described the changes in central metabolism and respiration that occur over the course of a yeast respiratory oscillation (15, 57, 59, 60) and recent evidence suggests that this temporal organization of metabolism optimizes cellular processes in a manner that confers stress resistance (61). Among genes that show the highest periodicity in the yeast respiratory oscillation are COX10, involved in heme *a* biosynthesis (a pathway that converts heme *b* to heme *a* via a stable heme *o* intermediate) (57, 62), and PET117, involved in assembly of the mitochondrial (aa_3-type) terminal oxidase (63). Interestingly, the *cyo* operon, which showed strong periodicity and upregulation in biomass that forms in the light under light/dark and temperature cycling conditions, includes the heme *o*/*a* biosynthetic gene *cyoE*. The

P. aeruginosa aa_3-type oxidase also showed periodicity and upregulation in biomass that forms in the light under cycling conditions. Thus, in both yeast and *P. aeruginosa*, periodicity of these genes during respiratory oscillations and growth in cycling conditions likely reflect increased demand for the terminal oxidases that use *a*- and *o*-type hemes, i.e., Cox/mitochondrial terminal oxidase and the Cyo terminal oxidase.

Microbial physiology can be sensitized to light exposure when (i) light damages cofactors that are required for protein function (11, 32, 33, 35, 64, 65), or (ii) when light stimulates a conformational change in a protein that participates in regulatory interactions (55, 66–68). Yeast respiratory oscillations occur in the absence of light/dark cycling but show altered period and amplitude during constant exposure to blue light. These effects appear to arise from light-dependent inhibition of respiratory cytochromes, which show absorption peaks that correlate with wavelengths that have the greatest impacts on the oscillations (12). While a similar inhibition could contribute to the fluctuation in respiratory activity reported here, which occurs in *P. aeruginosa* biofilms grown under light/dark cycling, our observations indicate that it is not the sole elicitor of this pattern. First, the formation of rings of reduced TTC occurs in *P. aeruginosa* biofilms grown in cycling conditions with blue, red, or far-red light and is not specific to wavelengths that are maximally absorbed by cytochromes. Second, we identified proteins with potential regulatory functions that contribute to ring formation. The first of these, BphP, is a light-sensing histidine kinase that contains the N-terminal phytochrome domain architecture characteristic of these proteins. BphP has previously been shown to affect regulatory cascades and biofilm development in response to light (18, 29). The second, PtsP, is a phosphotransferase that contains an N-terminal GAF domain. GAF domains are common sensory domains that can detect a broad range of stimuli and that are associated with light sensing in proteins from diverse organisms. PtsP is part of a signaling network that controls diverse processes, including aspects of central metabolism, in pseudomonads and other bacteria (69). Notably, although the protein RmcA makes a strong contribution to morphological changes in light-exposed biofilms (70), we found that the Δ*phz*Δ*rmcA* mutant showed a TTC reduction phenotype similar to that of the parent strain when grown under light/dark cycling conditions. Overall, the results of our study are consistent with a model in which light affects respiratory activity both through effects of specific wavelengths on cytochromes in the electron transport chain and effects on the conformation of light-sensing regulatory proteins.

In soil and aquatic environments, *P. aeruginosa* is typically found associated with eukaryotic organisms or in sites that have been contaminated by human activity (71). It can also colonize a broad range of hosts (72–75). In humans, *P. aeruginosa* can cause a variety of infections, including pneumonia, sepsis, and skin and soft tissue infections. In many of the diverse settings it can inhabit, *P. aeruginosa* has the potential to experience direct exposure to light or the effect of light on host physiology. Light

entrains host circadian rhythms, which include fluctuations in body temperature and variations in immune system function (76, 77). By responding to light/dark and temperature cycling, *P. aeruginosa* might have the ability to tune its physiology for optimal survival during association with hosts. A similar capability has been proposed for the commensal enteric bacterium *Klebsiella aerogenes*, which shows rhythmic gene expression that is entrained by temperature changes comparable to those seen for human body temperature (51, 78, 79). A better understanding of the effects of light/dark and temperature cycling on pathogen physiology could aid in the development of treatment approaches, which could, for example, be timed to maximize their effects or augmented by modification of light and temperature parameters in situ.

MATERIALS AND METHODS

Bacterial culture and light/dark cycling assay

All species and strains used in this study are listed in **Table S1A**. For light/dark (L/D) cycling assays, 1% tryptone (Teknova) plus 1.25% agar (Teknova) was autoclaved and allowed to cool to 60 ˚C and optionally amended with 0.001% to 0.005% 2,3,5-triphenyltetrazolium chloride (TTC) (Sigma Aldrich, Cat # T8877), depending on experimental procedure. Portions (90 ml) of the agar mixture were poured into UV-sterilized, square, gridless plates (Greiner Bio-One, Cat # 688102) and after agar plates solidified they were stored in a dark chamber at 25 ˚C overnight (14 h to 24 h). Bacterial liquid cultures (3 ml of lysogeny broth (LB; (80))) were inoculated using single colonies and shaken at 250 rpm at 37 ˚C overnight (12 h to 16 h). Subcultures were prepared by diluting overnight cultures 1:100 into 3 ml of LB and grown at 37 ˚C with shaking (250 rpm) until mid-exponential phase was reached (0.4 to 0.6 AU absorbance measurements at 500 nm, OD_{500}). Agar plates were dried in a ventilated, sterile biosafety cabinet for 60 min. One or 5 µl of subculture were spotted onto agar plates. Colonies on agar plates were placed in a temperature-controlled (0.2 ˚C error) incubator with a fitted lighting system (Percival Scientific CU-22LC9). Colony biofilms were grown at 25 ˚C (unless otherwise indicated) at 90-100% humidity for 6 days (or specified if longer) under various lighting conditions (specified below). Images were taken with a Zeiss AxioZoom.V16 Fluorescence zoom Stereomicroscope fitted with an iPod camera or as time-lapse movies using a custom-built movie chamber as described in (18). Time-lapse images were acquired every 30 min. All images were taken in the dark to ensure that the pixel values in the images were consistent.

Light conditions for light/dark cycling experiments

For most light/dark cycling experiments white light exposure (bulbs: F17T8/TL841/ALTO, Philips) was calibrated to 68.64 µmol photons m^{-2} s^{-1}. Light intensities were measured as photon flux density between 400 nm and 700 nm using an AMOUR-SL-125-PAR meter (Biospherical Instruments) for all light bulbs except the far-red light bulbs. For the wavelength-specific light exposure experiments (**Figure 5**), blue light photon flux density (bulbs: ELA-085, F17T8/BL-450, Percival Scientific) was set to 22.1 µmol m^{-2} s^{-1}, and red light photon flux density (bulbs: ELA-086, F17T8/IR-660, Percival Scientific) was set to 40 µmol m^{-2} s^{-1}. Light intensities for peak wavelengths of all light bulbs were measured using an S130C photodiode power sensor (Thorlabs) with a PM100A power meter console (Thorlabs). For comparison between light bulbs, white light flux density (analyzed at 436, 545, and 612 nm) was measured as 2.66, 1.31, and 1 W/m^2, respectively. Blue light flux density (analyzed at 422 nm) was measured as 1.11 W/m^2, red light flux density (analyzed at 660 nm) was measured as 0.87 W/m^2, and far-red light flux density (analyzed at 750 nm; bulbs: ELA-087, F17T8/IR-750, Percival Scientific) was measured as 0.87 W/m^2. For the majority of experiments light/dark cycles were set to a 24-hour period (12 hours of light and 12 hours of dark). For experiments with shortened and prolonged light/dark cycles (**Figure 2**), periods were set to 12 hours (6 hours of light at 25 ˚C and 6 hours of dark at 23 ˚C) or 48 hours (24 hours of light at 25 ˚C and 24 hours of dark at 23 ˚C).

Exposure to TTC post-completion of light/dark cycling assay

For exposure of mature biofilms to TTC (**Figure 4B**), agar plates were prepared as for other light/dark cycling experiments except that the growth medium was not amended with TTC. Bacterial liquid cultures of Δ*phz* Δ*pel* mutants were prepared as described above and spotted on Whatman filter disks. Bacterial colonies were grown under the following cycling conditions: 12-hour white light exposure at 25 ˚C, followed by 12-hour dark at 23 ˚C. Five days after the colonies were spotted, tryptone agar plates were prepared and amended with 0.005% TTC. After 6 days of growth, biofilms were transferred to TTC-amended tryptone agar by carefully lifting each filter disk and placing it on the agar. Images of TTC reduction were taken every 30 or 60 min (final image after 270 min) using the AxioZoom setup as described above.

Deletion mutants and gfp-*expression mutants*

Markerless gene deletions were created as described in (17). Combinatorial deletion mutants were constructed by successive single deletions of respective genes. Deletion mutants in *P. aeruginosa* PA14 are listed in **Table S1A**. Primers used to amplify 1 kb of flanking sequence from each side of the target gene are listed in **Table S1B**. Plasmids harboring the gene deletion constructs are listed in **Table S1C**.

RNA sequencing (RNAseq) and transcriptomic analysis

Biofilms were grown in light/dark cycling with 2˚C temperature changes (light/25˚C vs. dark/23˚C in 12-hour intervals) on 0.22 µm polypropylene filters atop agar-solidified medium for 76 hours. The growth medium was 1% tryptone plus 1% agar amended with 0.0025% TTC. Prior to sample collection, each biofilm was placed on a slide with 100 µl RNAlater (Thermo Fisher). Samples were collected by laser capture microdissection microscopy using a Zeiss PALM MicroBeam IV from the outermost four rings (two red rings, i.e., Dark 1 and Dark 2, and the two white rings, i.e., Light 1 and Light 2) for two separate colony biofilms. Areas of the biofilms ranging from 1 to 10 mm^2 were dissected and transferred to tubes containing 200 µl RNAlater (Thermofisher). Samples were homogenized using a motorized pestle and total RNA was extracted and purified using a RNeasy Plant Mini Kit and RNeasy MinElute Cleanup Kit (Qiagen). RNA was sent to GENEWIZ, Inc. for sequencing with Illumina HiSeq. Reads were mapped using Geneious Prime 2022.0 (https://www.geneious.com) and differential gene expression was determined (method: Geneious; transcripts were normalized by median of gene expression ratios). The heatmap was generated using the R packages ComplexHeatmap, RColorBrewer, and circlize by scaling log-transformed normalized counts by row (gene). Dimension reduction was performed by principal component analysis (depicted in **Figure S4**) using the R package DESeq2. Significant (adjusted *p*-value < 0.05) and highly differentially expressed ($|\log_2 FC| > 1$) genes were visualized in the volcano plot (**Figure 6B**). Gene expression data were arranged into metabolic pathway groupings using the *P. aeruginosa* UCBPP-PA14 specific entry in the KEGG database (www.kegg.jp) (36) and the R package KEGGREST, and enrichment analysis was performed using the R package clusterProfiler.

Colony biofilm growth and TTC reduction: movie analysis

All RGB movie images were converted to grayscale. The 2D agar/colony boundary was determined for each image using a thresholding approach: Initially, the final movie image was used to approximate the agar/colony boundary and determine the average pixel intensity value for the entire agar area. Then, a Python script (**Supplemental file 2**), was used to scan from the agar area toward the edge of the colony. The agar/colony boundary was defined by a change in pixel intensity that exceeded three standard deviations from the average agar intensity. The intensity value at the agar/colony boundary in the final image was then used as the threshold to analyze all images and the time at which each pixel gained the threshold intensity was determined. Subsequent intensities were recorded and yielded data that allowed for the generation of TTC reduction graphs (**Figures 3B and 7C**).

ACKNOWLEDGEMENTS

This work was supported by NIH/NIAID grant R01AI103369 and NSF award 1553023 to L.D. Colony biofilm samples were collected by laser capture microdissection at the Confocal and Specialized Microscopy Shared Resource of the Herbert Irving Comprehensive Cancer Center at Columbia University, supported by NIH/NCI grant P30CA013696.

FIGURE LEGENDS

Figure 1. *Pseudomonas aeruginosa* Δ*phz* biofilms grown under light/dark or temperature cycling conditions form patterns of TTC reduction. (A) Schematic showing PA14 electron transport chain (ETC)-dependent reduction of TTC, which produces a red precipitate. **(B)** Schematic of experimental setup examining the effect of biofilm growth under constant or cycling conditions (with light or dark conditions indicated by the sun and moon). **(C-G)** Left: Δ*phz* biofilm grown with the indicated conditions. Right: quantification of red color intensity (i.e. TTC reduction) at the indicated distance from the biofilm center for a radius of the biofilm. The concentration of TTC in the growth medium was 0.004%. Experiments were performed with biological triplicates and representative data are shown. Scale bars are 2.5 mm.

Figure 2. TTC reduction patterns respond to altered periods of light/dark and temperature cycling. Biofilms grown under light/dark and 25˚C/23˚C cycling conditions with 6-hour (left panel), 12-hour (middle panel), or 24-hour (right panel) alternating intervals. The concentration of TTC in the growth medium was 0.004%. Quantification of the final pixel intensity for a radius of each biofilm is shown in the bottom panels. Experiments were performed with biological triplicates and representative data are shown.

Figure 3. Conditions present during formation of each biofilm growth ring affect the total TTC reduced by the ring. (A) Kymograph showing pixel coloration over time across a radius of a biofilm (as depicted in the drawing) grown with light/dark and 25˚C/23˚C cycling conditions on medium containing 0.004% TTC. Bars labeled “A”-”D” indicate the points at which biomass became detectable via image analysis. **(B)** Reduced TTC quantified as average pixel value over time for each ring of growth of the biofilm shown in (A). “A””D” labeling corresponds to pixels of biomass becoming detectable as indicated in (A). Traces corresponding to biomass appearing during dark intervals are shown in shades of blue; those corresponding to biomass appearing during light intervals are shown in shades of yellow. Traces that initiate in dark or light intervals are shown on separate plots, for clarity, at right.

Figure 4. Fixed physiological states are maintained after growth in cycling conditions. (A) Model of biofilm development under cycling conditions: The environmental condition (e.g., light or dark) experienced by perceptive cells at the leading edge of the biofilm (blue) "sets" their physiological status, which then remains fixed through subsequent changes in conditions. **(B)** Left panels: Biofilm coloration after 144 hours of growth under light/dark and 25˚C/23˚C cycling conditions on medium without TTC ("0 min"), and then after transfer to medium containing 0.005% TTC and incubation under constant dark and 23˚C conditions for 270 min. Right panel: Quantification of pixel intensity across a selected radius, at the indicated time points, for the biofilm shown at left.

Figure 5. Biofilms grown under light/dark cycling conditions form TTC reduction patterns in blue, red, or far-red light, and Δ*bphP* and Δ*ptsP* mutants show defects in TTC ring pattern formation specifically under red light. TTC reduction patterns in biofilms of the parent strain (Δ*phz*) and indicated mutants grown under light/dark cycling of blue, red, or far-red light with 12-hour intervals. Temperature was kept constant at 25˚C and the growth medium contained 0.004% TTC. Experiments were performed with biological triplicates and representative data are shown.

Figure 6. Fixed physiological responses in biofilms grown with light/dark and temperature cycling are evident in differences in transcription. (A) Top: Schematic showing sampling sites in a biofilm grown under cycling conditions on medium containing TTC. The indicated biofilm zones were sampled from duplicate biofilms and subjected to RNAseq. Bottom: Heatmaps representing relative transcript levels (z-scores), shown for each replicate biofilm sample in order of fold change. One sample was omitted because it was determined to be an outlier by principal component analysis. **(B)** Volcano plot showing $\log_2$-transformed average fold change versus statistical significance for each gene, based on normalized transcript levels detected by RNAseq in biofilm zones formed during light vs. dark intervals. Genes that showed a >2-fold increase in expression under dark/23˚C or light/25˚C conditions are represented in blue or yellow, respectively. A total of 5945 genes are represented. **(C)** Gene set enrichment analysis using groups of genes based on KEGG-annotated metabolic pathways. Significant enrichment scores above 0 correspond to over-represented groups of genes in biofilm zones from light intervals, while significant enrichment scores below 0 correspond to over-represented groups of genes in biofilm zones from dark intervals. Gene ratio corresponds to the fraction of genes per pathway contributing to the enrichment.

Figure 7. Light/dark and temperature cycling affects the expression of PA14 terminal oxidase genes and *cbb*$_3$-type oxidases influence the dynamics of biofilm TTC reduction under this condition. (A) Average relative expression of representative genes that code for subunits of terminal

oxidase complexes (source: RNAseq analysis in **Figure 6**). “L1” refers to the “Light 1” ring depicted in Figure 6A (Top), “D1” refers to the “Dark 1” ring, and so on. Error bars indicate the standard deviation of duplicate samples. **(B)** Schematic of *P. aeruginosa*’s branched ETC. Cyo, Cio, Cox, Cco2, and Cco1 are terminal oxidase complexes and Cco4 refers to two “orphan” terminal oxidase subunits that can replace the corresponding subunits in Cco2 or Cco1 (17, 41). **(C)** Pixel intensity over time for selected pixels in biofilms of the indicated strains grown under light/dark and temperature cycling on medium containing 0.004% TTC. **(D)** TTC reduction rate over time for data shown in (C), with data for biomass that formed under dark conditions at left and data for biomass that formed under light conditions at right. For (C) and (D), Data points for biomass formed under dark conditions are blue and those for biomass formed under light conditions are yellow. Darker shades of blue and yellow are used for biomass that formed at earlier time points within an interval and lighter shades are used for biomass that formed at later time points. Results are representative of 3 biological replicates.

SUPPLEMENTAL MATERIAL

Figure S1. Schematic showing the structure and reduction of TTC.

Figure S2. Growth of colony biofilms on medium containing 0.004% TTC under constant dark or light conditions with cycling between 12 hours at 23˚C and 12 hours at 25˚C.

Figure S3. Schematic of incubation setup used to generate time-lapse movies of colony biofilm growth and TTC reduction.

Figure S4. Dimensionality reduction by principal component analysis was applied to RNAseq data for the full set of 8 samples obtained as shown in Figure 6A (Top). Maximum possible variance was accounted for by the first two principle components PC1 and PC2. Each sample is plotted according to its values for PC1 and PC2.

Figure S5. (A) Sixty-seven percent of genes involved in the pentose phosphate pathway were identified in the RNAseq as showing differential expression in biomass formed under light/dark and temperature cycling. Genes coding for enzymes involved in the oxidative branch were upregulated in biomass that formed under light/25˚C conditions, and genes coding for enzymes involved in the non-oxidative branch were upregulated in biomass that formed under dark/23˚C conditions. The heatmap shows genes involved in the pentose phosphate pathway, arranged according to their relative periodicity in samples from biomass formed under light/dark and temperature cycling. **(B)** Schematic of the pentose phosphate pathway highlighting selected genes whose expression was affected by growth

under light/dark and temperature cycling conditions.

Figure S6. Images of Δ*phz*, Δ*phz*Δ*cco1cco2*, and Δ*phz* PaCco1 colony biofilms, corresponding to the analyses shown in Figure 7C and D.

Table S1A. Strains used in this study

Table S1B. Primers used in this study

Table S1C. Plasmids used in this study

Supplemental file 1. List of RNAseq genes

Supplemental file 2. Python code for colony time-lapse imaging

REFERENCES

1. Soo RM, Hemp J, Parks DH, Fischer WW, Hugenholtz P. 2017. On the origins of oxygenic photosynthesis and aerobic respiration in Cyanobacteria. Science 355:1436–1440.

2. Canfield DE, Des Marais DJ. 1993. Biogeochemical cycles of carbon, sulfur, and free oxygen in a microbial mat. Geochim Cosmochim Acta 57:3971–3984.

3. Gerhardt S, Brune A, Schink B. 2005. Dynamics of Redox Changes of Iron Caused by Light–dark Variations in Littoral Sediment of a Freshwater Lake. Biogeochemistry 74:323–339.

4. Mulholland PJ, Houser JN, Maloney KO. 2005. Stream diurnal dissolved oxygen profiles as indicators of in-stream metabolism and disturbance effects: Fort Benning as a case study. Ecol Indic 5:243–252.

5. Dorau K, Bohn B, Weihermüller L, Mansfeldt T. 2021. Temperature-induced diurnal redox potential in soil. Environ Sci Process Impacts 23:1782–1790.

6. Huus KE, Ley RE. 2021. Blowing Hot and Cold: Body Temperature and the Microbiome. mSystems 6:e0070721.

7. Coiffard B, Diallo AB, Mezouar S, Leone M, Mege J-L. 2021. A Tangled Threesome: Circadian Rhythm, Body Temperature Variations, and the Immune System. Biology 10.

8. Refinetti R. 2020. Circadian rhythmicity of body temperature and metabolism. Temperature (Austin) 7:321–362.

9. Pearson JA, Voisey AC, Boest-Bjerg K, Wong FS, Wen L. 2021. Circadian Rhythm Modulation of Microbes During Health and Infection. Front Microbiol 12:721004.

10. Hameed A, Lai W-A, Shahina M, Stothard P, Young L-S, Lin S-Y, Sridhar KR, Young C-C. 2020. Differential visible spectral influence on carbon metabolism in heterotrophic marine flavobacteria. FEMS Microbiol Ecol 96.

11. D'Aoust JY, Giroux J, Baraan LR, Schneider H, Martin WG. 1974. Some effects of visible light on Escherichia coli. J Bacteriol 120:799–804.

12. Robertson JB, Davis CR, Johnson CH. 2013. Visible light alters yeast metabolic rhythms by inhibiting respiration. Proc Natl Acad Sci U S A 110:21130–21135.

13. Yang C-Y, Bialecka-Fornal M, Weatherwax C, Larkin JW, Prindle A, Liu J, Garcia-Ojalvo J, Süel

GM. 2020. Encoding Membrane-Potential-Based Memory within a Microbial Community. Cell Syst 10:417–423.e3.

14. Edgar RS, Green EW, Zhao Y, van Ooijen G, Olmedo M, Qin X, Xu Y, Pan M, Valekunja UK, Feeney KA, Maywood ES, Hastings MH, Baliga NS, Merrow M, Millar AJ, Johnson CH, Kyriacou CP, O'Neill JS, Reddy AB. 2012. Peroxiredoxins are conserved markers of circadian rhythms. Nature 485:459–464.

15. Causton HC, Feeney KA, Ziegler CA, O'Neill JS. 2015. Metabolic Cycles in Yeast Share Features Conserved among Circadian Rhythms. Curr Biol 25:1056–1062.

16. Dietrich LEP, Okegbe C, Price-Whelan A, Sakhtah H, Hunter RC, Newman DK. 2013. Bacterial community morphogenesis is intimately linked to the intracellular redox state. J Bacteriol 195:1371–1380.

17. Jo J, Cortez KL, Cornell WC, Price-Whelan A, Dietrich LE. 2017. An orphan cbb3-type cytochrome oxidase subunit supports Pseudomonas aeruginosa biofilm growth and virulence. Elife 6:171538.

18. Kahl LJ, Price-Whelan A, Dietrich LEP. 2020. Light-Mediated Decreases in Cyclic di-GMP Levels Inhibit Structure Formation in Pseudomonas aeruginosa Biofilms. J Bacteriol 202.

19. Tanaka J, Kiyoshi K, Kadokura T, Suzuki K-I, Nakayama S. 2021. Elucidation of the enzyme involved in 2,3,5-triphenyl tetrazolium chloride (TTC) staining activity and the relationship between TTC staining activity and fermentation profiles in Saccharomyces cerevisiae. J Biosci Bioeng 131:396–404.

20. Hurwitz SJ, McCarthy TJ. 1986. 2,3,5-Triphenyltetrazolium chloride as a novel tool in germicide dynamics. J Pharm Sci 75:912–916.

21. Rich PR, Mischis LA, Purton S, Wiskich JT. 2001. The sites of interaction of triphenyltetrazolium chloride with mitochondrial respiratory chains. FEMS Microbiol Lett 202:181–187.

22. Larney FJ, Blackshaw RE. 2003. Weed seed viability in composted beef cattle feedlot manure. J Environ Qual 32:1105–1113.

23. Kern SE, Price-Whelan A, Newman DK. 2014. Extraction and measurement of NAD(P)(+) and NAD(P)H. Methods Mol Biol 1149:311–323.

24. Pfeifroth U, Sanchez-Lorenzo A, Manara V, Trentmann J, Hollmann R. 2018. Trends and variability of surface solar radiation in Europe based on surface- and satellite-based data records. J Geophys Res https://doi.org/10.1002/2017jd027418.

25. Salomon M, Christie JM, Knieb E, Lempert U, Briggs WR. 2000. Photochemical and mutational analysis of the FMN-binding domains of the plant blue light receptor, phototropin. Biochemistry 39:9401–9410.

26. Swartz TE, Tseng TS, Frederickson MA, Paris G, Comerci DJ, Rajashekara G, Kim JG, Mudgett MB, Splitter GA, Ugalde RA, Goldbaum FA, Briggs WR, Bogomolni RA. 2007. Blue-light-activated histidine kinases: Two-component sensors in bacteria. Science 317:1090–1093.

27. Bieszke JA, Braun EL, Bean LE, Kang S, Natvig DO, Borkovich KA. 1999. The nop-1 gene of Neurospora crassa encodes a seven transmembrane helix retinal-binding protein homologous to archaeal rhodopsins. Proc Natl Acad Sci U S A 96:8034–8039.

28. De Luca G, Fochesato S, Lavergne J, Forest KT, Barakat M, Ortet P, Achouak W, Heulin T, Verméglio A. 2019. Light on the cell cycle of the non-photosynthetic bacterium Ramlibacter tataouinensis. Sci Rep 9:16505.

29. Mukherjee S, Jemielita M, Stergioula V, Tikhonov M, Bassler BL. 2019. Photosensing and quorum sensing are integrated to control Pseudomonas aeruginosa collective behaviors. PLoS Biol 17:e3000579.

30. Aravind L, Ponting CP. 1997. The GAF domain: an evolutionary link between diverse phototransducing proteins. Trends Biochem Sci 22:458–459.

31. Zoltowski BD, Gardner KH. 2011. Tripping the light fantastic: blue-light photoreceptors as examples of environmentally modulated protein-protein interactions. Biochemistry 50:4–16.

32. Epel B, Butler WL. 1969. Cytochrome a3: destruction by light. Science 166:621–622.

33. Ninnemann H. 1972. Photoinhibition of respiration in bacteria and the cyanophycea Vitreoscilla stercoraria. FEBS Lett 27:179–180.

34. Hessling M, Spellerberg B, Hoenes K. 2017. Photoinactivation of bacteria by endogenous photosensitizers and exposure to visible light of different wavelengths - a review on existing data. FEMS Microbiol Lett 364.

35. Plavskii VY, Mikulich AV, Tretyakova AI, Leusenka IA, Plavskaya LG, Kazyuchits OA, Dobysh II, Krasnenkova TP. 2018. Porphyrins and flavins as endogenous acceptors of optical radiation of blue spectral region determining photoinactivation of microbial cells. J Photochem Photobiol B 183:172–183.

36. Kanehisa M, Furumichi M, Sato Y, Ishiguro-Watanabe M, Tanabe M. 2021. KEGG: integrating

viruses and cellular organisms. Nucleic Acids Res 49:D545–D551.

37. Kawakami T, Kuroki M, Ishii M, Igarashi Y, Arai H. 2010. Differential expression of multiple terminal oxidases for aerobic respiration in Pseudomonas aeruginosa. Environ Microbiol 12:1399–1412.

38. Milev NB, Rhee S-G, Reddy AB. 2018. Cellular Timekeeping: It's Redox o'Clock. Cold Spring Harb Perspect Biol 10.

39. de Goede P, Wefers J, Brombacher EC, Schrauwen P, Kalsbeek A. 2018. Circadian rhythms in mitochondrial respiration. J Mol Endocrinol 60:R115–R130.

40. Reinke H, Asher G. 2019. Crosstalk between metabolism and circadian clocks. Nat Rev Mol Cell Biol 20:227–241.

41. Hirai T, Osamura T, Ishii M, Arai H. 2016. Expression of multiple cbb3 cytochrome c oxidase isoforms by combinations of multiple isosubunits in Pseudomonas aeruginosa. Proc Natl Acad Sci U S A 113:12815–12819.

42. Arai H, Kawakami T, Osamura T, Hirai T, Sakai Y, Ishii M. 2014. Enzymatic characterization and in vivo function of five terminal oxidases in Pseudomonas aeruginosa. J Bacteriol 196:4206–4215.

43. Stal LJ. 2001. Coastal microbial mats: the physiology of a small-scale ecosystem. S Afr J Bot 67:399–410.

44. Ottesen EA, Young CR, Gifford SM, Eppley JM, Marin R 3rd, Schuster SC, Scholin CA, DeLong EF. 2014. Ocean microbes. Multispecies diel transcriptional oscillations in open ocean heterotrophic bacterial assemblages. Science 345:207–212.

45. Badri DV, Vivanco JM. 2009. Regulation and function of root exudates. Plant Cell Environ 32:666–681.

46. Gyöngyösi N, Káldi K. 2014. Interconnections of reactive oxygen species homeostasis and circadian rhythm in Neurospora crassa. Antioxid Redox Signal 20:3007–3023.

47. Chou K-T, Lee D-YD, Chiou J-G, Galera-Laporta L, Ly S, Garcia-Ojalvo J, Süel GM. 2022. A segmentation clock patterns cellular differentiation in a bacterial biofilm. Cell 185:145–157.e13.

48. Eelderink-Chen Z, Bosman J, Sartor F, Dodd AN, Kovács ÁT, Merrow M. 2021. A circadian clock in a nonphotosynthetic prokaryote. Science Advances 7:eabe2086.

49. Soriano MI, Roibás B, García AB, Espinosa-Urgel M. 2010. Evidence of circadian rhythms in non-

photosynthetic bacteria? J Circadian Rhythms 8:8.

50. Tiensuu T, Andersson C, Rydén P, Johansson J. 2013. Cycles of light and dark co-ordinate reversible colony differentiation in Listeria monocytogenes. Mol Microbiol 87:909–924.

51. Paulose JK, Wright JM, Patel AG, Cassone VM. 2016. Human Gut Bacteria Are Sensitive to Melatonin and Express Endogenous Circadian Rhythmicity. PLoS One 11:e0146643.

52. Okamoto S, Furuya K, Nozaki S, Aoki K, Niki H. 2013. Synchronous activation of cell division by light or temperature stimuli in the dimorphic yeast Schizosaccharomyces japonicus. Eukaryot Cell 12:1235–1243.

53. Franco DL, Canessa P, Bellora N, Risau-Gusman S, Olivares-Yañez C, Pérez-Lara R, Libkind D, Larrondo LF, Marpegan L. 2017. Spontaneous circadian rhythms in a cold-adapted natural isolate of Aureobasidium pullulans. Sci Rep 7:13837.

54. Saha R, Liu D, Hoynes-O'Connor A, Liberton M, Yu J, Bhattacharyya-Pakrasi M, Balassy A, Zhang F, Moon TS, Maranas CD, Pakrasi HB. 2016. Diurnal Regulation of Cellular Processes in the Cyanobacterium *Synechocystis* sp. Strain PCC 6803: Insights from Transcriptomic, Fluxomic, and Physiological Analyses. MBio 7.

55. Purcell EB, Crosson S. 2008. Photoregulation in prokaryotes. Curr Opin Microbiol 11:168–178.

56. Chen Yi-Bu, Dominic Benny, Mellon Mark T., Zehr Jonathan P. 1998. Circadian Rhythm of Nitrogenase Gene Expression in the Diazotrophic Filamentous Nonheterocystous CyanobacteriumTrichodesmium sp. Strain IMS 101. J Bacteriol 180:3598–3605.

57. Tu BP, Kudlicki A, Rowicka M, McKnight SL. 2005. Logic of the yeast metabolic cycle: temporal compartmentalization of cellular processes. Science 310:1152–1158.

58. Whitehead K, Pan M, Masumura K-I, Bonneau R, Baliga NS. 2009. Diurnally entrained anticipatory behavior in archaea. PLoS One 4:e5485.

59. Tu BP, McKnight SL. 2007. The yeast metabolic cycle: insights into the life of a eukaryotic cell. Cold Spring Harb Symp Quant Biol 72:339–343.

60. Baumgartner BL, O'Laughlin R, Jin M, Tsimring LS, Hao N, Hasty J. 2018. Flavin-based metabolic cycles are integral features of growth and division in single yeast cells. Sci Rep 8:18045.

61. O'Neill JS. 2021. Redox-coupled rhythm and brews. Nat Chem Biol.

62. Hederstedt L. 2012. Heme A biosynthesis. Biochim Biophys Acta 1817:920–927.

63. Taylor NG, Swenson S, Harris NJ, Germany EM, Fox JL, Khalimonchuk O. 2017. The Assembly Factor Pet117 Couples Heme a Synthase Activity to Cytochrome Oxidase Assembly. J Biol Chem 292:1815–1825.

64. Ninnemann H. 1974. Photoinhibition of isolated complexes I, II, and 3 of beef heart mitochondria. FEBS Lett 39:353–358.

65. Schmid J, Hoenes K, Vatter P, Hessling M. 2019. Antimicrobial Effect of Visible Light-Photoinactivation of Legionella rubrilucens by Irradiation at 450, 470, and 620 nm. Antibiotics (Basel) 8.

66. Elías-Arnanz M, Padmanabhan S, Murillo FJ. 2011. Light-dependent gene regulation in nonphototrophic bacteria. Curr Opin Microbiol 14:128–135.

67. Fraikin GY, Strakhovskaya MG, Belenikina NS, Rubin AB. 2015. Bacterial photosensory proteins: Regulatory functions and optogenetic applications. Microbiology 84:461–472.

68. Losi A, Gärtner W. 2021. A light life together: photosensing in the plant microbiota. Photochem Photobiol Sci 20:451–473.

69. Pflüger-Grau K, de Lorenzo V. 2014. From the phosphoenolpyruvate phosphotransferase system to selfish metabolism: a story retraced in Pseudomonas putida. FEMS Microbiol Lett 356:144–153.

70. Kahl LJ, Price-Whelan A, Dietrich LEP. 2020. Light-mediated decreases in cyclic di-GMP levels inhibit structure formation in *Pseudomonas aeruginosa* biofilms. J Bacteriol https://doi.org/10.1128/JB.00117-20.

71. Crone S, Vives-Flórez M, Kvich L, Saunders AM, Malone M, Nicolaisen MH, Martínez-García E, Rojas-Acosta C, Catalina Gomez-Puerto M, Calum H, Whiteley M, Kolter R, Bjarnsholt T. 2020. The environmental occurrence of Pseudomonas aeruginosa. APMIS 128:220–231.

72. Tan MW, Mahajan-Miklos S, Ausubel FM. 1999. Killing of Caenorhabditis elegans by Pseudomonas aeruginosa used to model mammalian bacterial pathogenesis. Proc Natl Acad Sci U S A 96:715–720.

73. Starkey M, Rahme LG. 2009. Modeling Pseudomonas aeruginosa pathogenesis in plant hosts. Nat Protoc 4:117–124.

74. Apidianakis Y, Rahme LG. 2009. Drosophila melanogaster as a model host for studying

Pseudomonas aeruginosa infection. Nat Protoc 4:1285–1294.

75. Lorenz A, Pawar V, Häussler S, Weiss S. 2016. Insights into host-pathogen interactions from state-of-the-art animal models of respiratory Pseudomonas aeruginosa infections. FEBS Lett 590:3941–3959.

76. Harding C, Pompei F, Bordonaro SF, McGillicuddy DC, Burmistrov D, Sanchez LD. 2019. The daily, weekly, and seasonal cycles of body temperature analyzed at large scale. Chronobiol Int 36:1646–1657.

77. Costantini C, Renga G, Sellitto F, Borghi M, Stincardini C, Pariano M, Zelante T, Chiarotti F, Bartoli A, Mosci P, Romani L, Brancorsini S, Bellet MM. 2020. Microbes in the Era of Circadian Medicine. Front Cell Infect Microbiol 10:30.

78. Paulose JK, Cassone VM. 2016. The melatonin-sensitive circadian clock of the enteric bacterium *Enterobacter aerogenes*. Gut Microbes 7:424–427.

79. Paulose JK, Cassone CV, Graniczkowska KB, Cassone VM. 2019. Entrainment of the Circadian Clock of the Enteric Bacterium *Klebsiella aerogenes* by Temperature Cycles. iScience 19:1202–1213.

80. Bertani G. 2004. Lysogeny at mid-twentieth century: P1, P2, and other experimental systems. J Bacteriol 186:595–600.

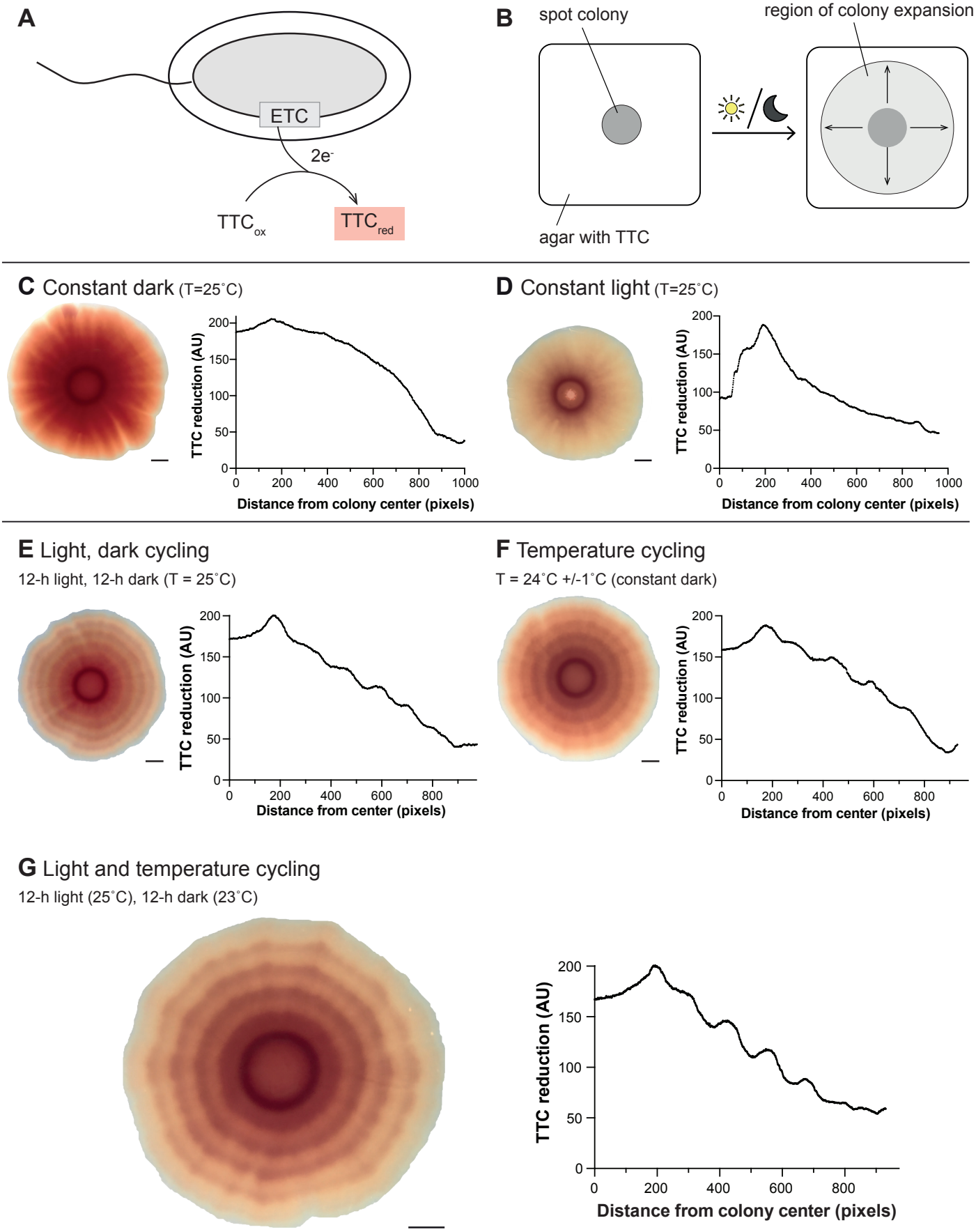
A
ETC
2e-
TTCox
TTCred
B
spot colony
region of colony expansion
agar with TTC
C Constant dark (T=25˚C)
TTC reduction (AU)
Distance from colony center (pixels)
D Constant light (T=25˚C)
TTC reduction (AU)
Distance from colony center (pixels)
E Light, dark cycling
12-h light, 12-h dark (T = 25˚C)
TTC reduction (AU)
Distance from center (pixels)
F Temperature cycling
T = 24˚C +/-1˚C (constant dark)
TTC reduction (AU)
Distance from center (pixels)
G Light and temperature cycling
12-h light (25˚C), 12-h dark (23˚C)
TTC reduction (AU)
Distance from colony center (pixels)

Figure 1. *Pseudomonas aeruginosa* Δ*phz* biofilms grown under light/dark or temperature cycling conditions form patterns of TTC reduction. (A) Schematic showing PA14 electron transport chain (ETC)-dependent reduction of TTC, which produces a red precipitate. **(B)** Schematic of experimental setup examining the effect of biofilm growth under constant or cycling conditions (with light or dark conditions indicated by the sun and moon). **(C-G)** Left: Δ*phz* biofilm grown with the indicated conditions. Right: quantification of red color intensity (i.e. TTC reduction) at the indicated distance from the biofilm center for a radius of the biofilm. The concentration of TTC in the growth medium was 0.004%. Experiments were performed with biological triplicates and representative data are shown. Scale bars are 2.5 mm.

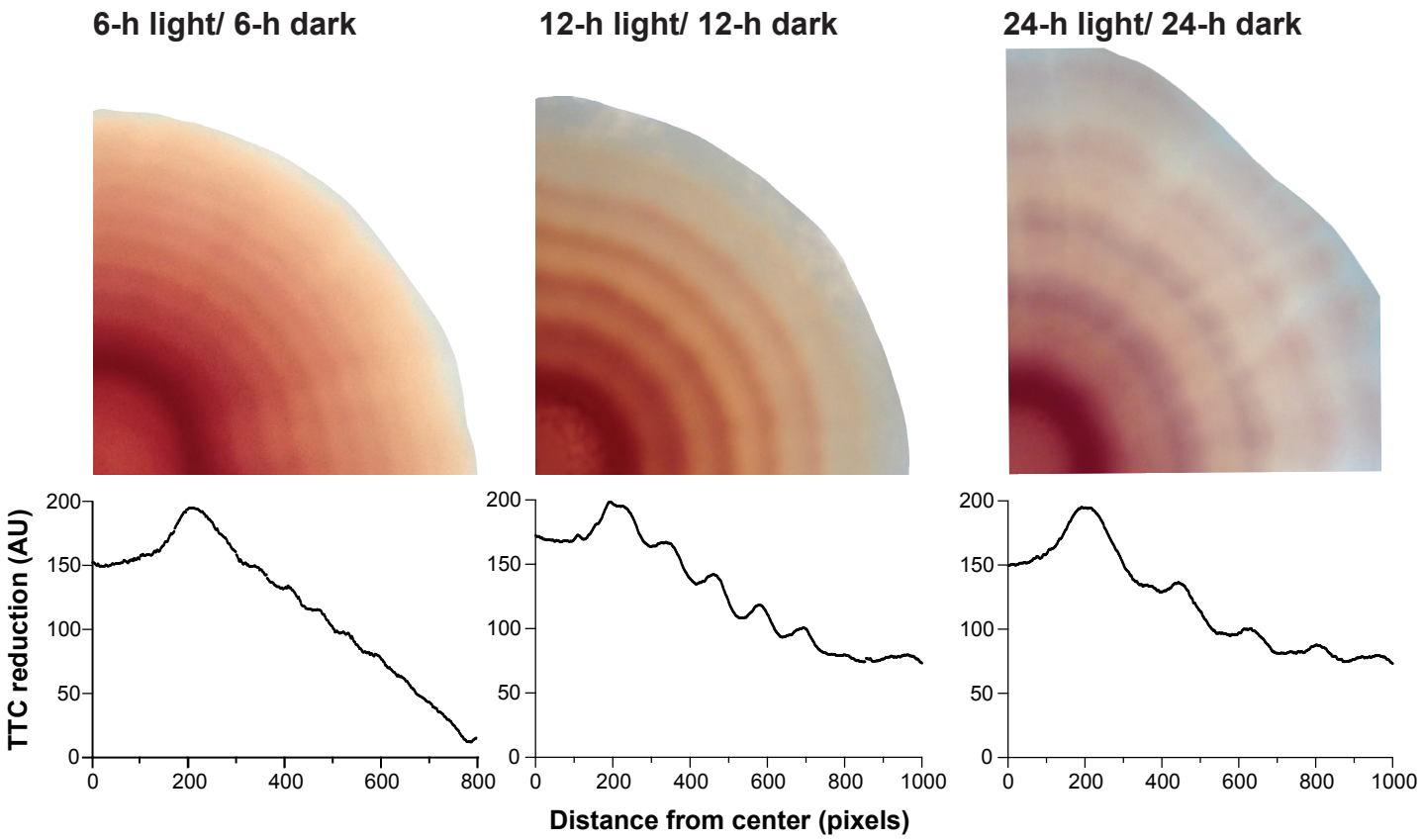

Figure 2. TTC reduction patterns respond to altered periods of light/dark and temperature cycling. Biofilms grown under light/dark and 25˚C/23˚C cycling conditions with 6-hour (left panel), 12-hour (middle panel), or 24-hour (right panel) alternating intervals. The concentration of TTC in the growth medium was 0.004%. Quantification of the final pixel intensity for a radius of each biofilm is shown in the bottom panels. Experiments were performed with biological triplicates and representative data are shown.

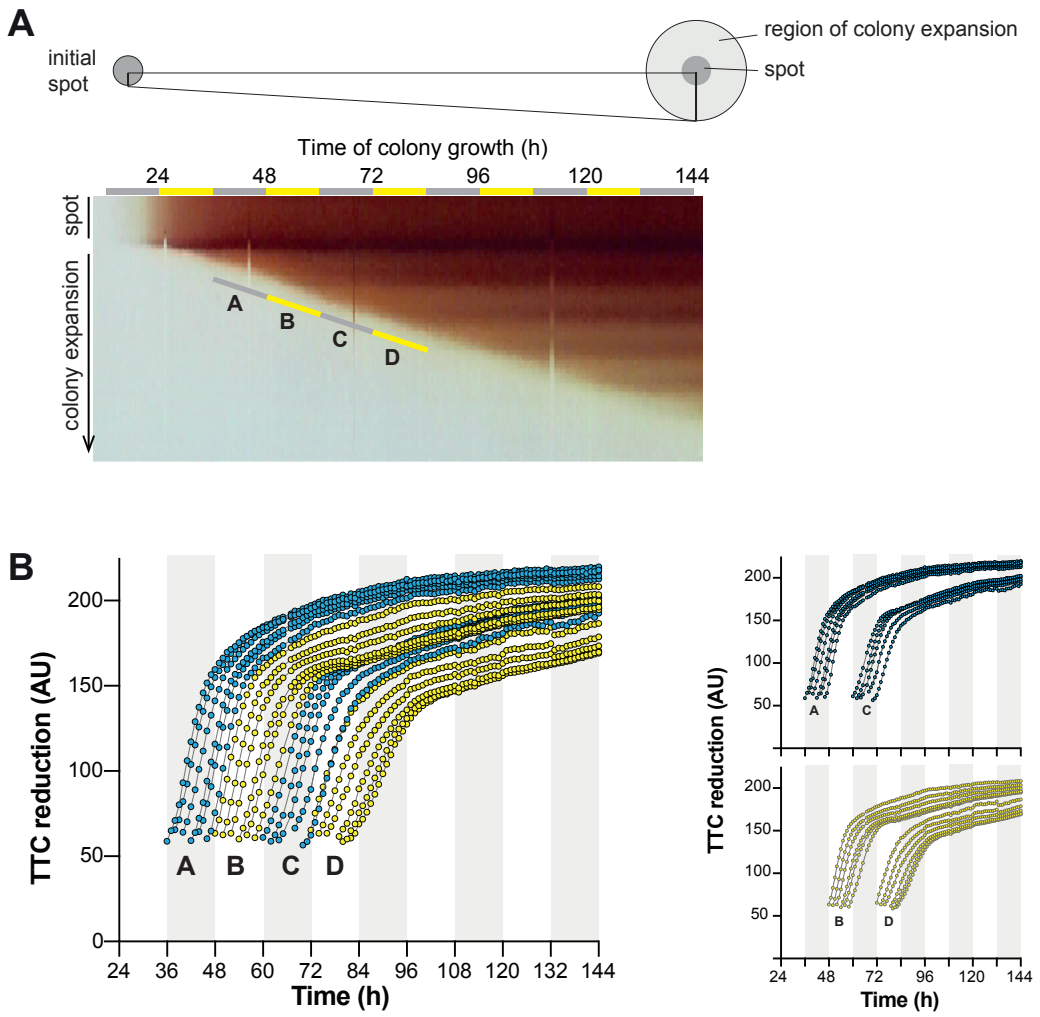

Figure 3. Conditions present during formation of each biofilm growth ring affect the total TTC reduced by the ring. (A) Kymograph showing pixel coloration over time across a radius of a biofilm (as depicted in the drawing) grown with light/dark and 25˚C/23˚C cycling conditions on medium containing 0.004% TTC. Bars labeled “A”-”D” indicate the points at which biomass became detectable via image analysis. **(B)** Reduced TTC quantified as average pixel value over time for each ring of growth of the biofilm shown in (A). “A””D” labeling corresponds to pixels of biomass becoming detectable as indicated in (A). Traces corresponding to biomass appearing during dark intervals are shown in shades of blue; those corresponding to biomass appearing during light intervals are shown in shades of yellow. Traces that initiate in dark or light intervals are shown on separate plots, for clarity, at right.

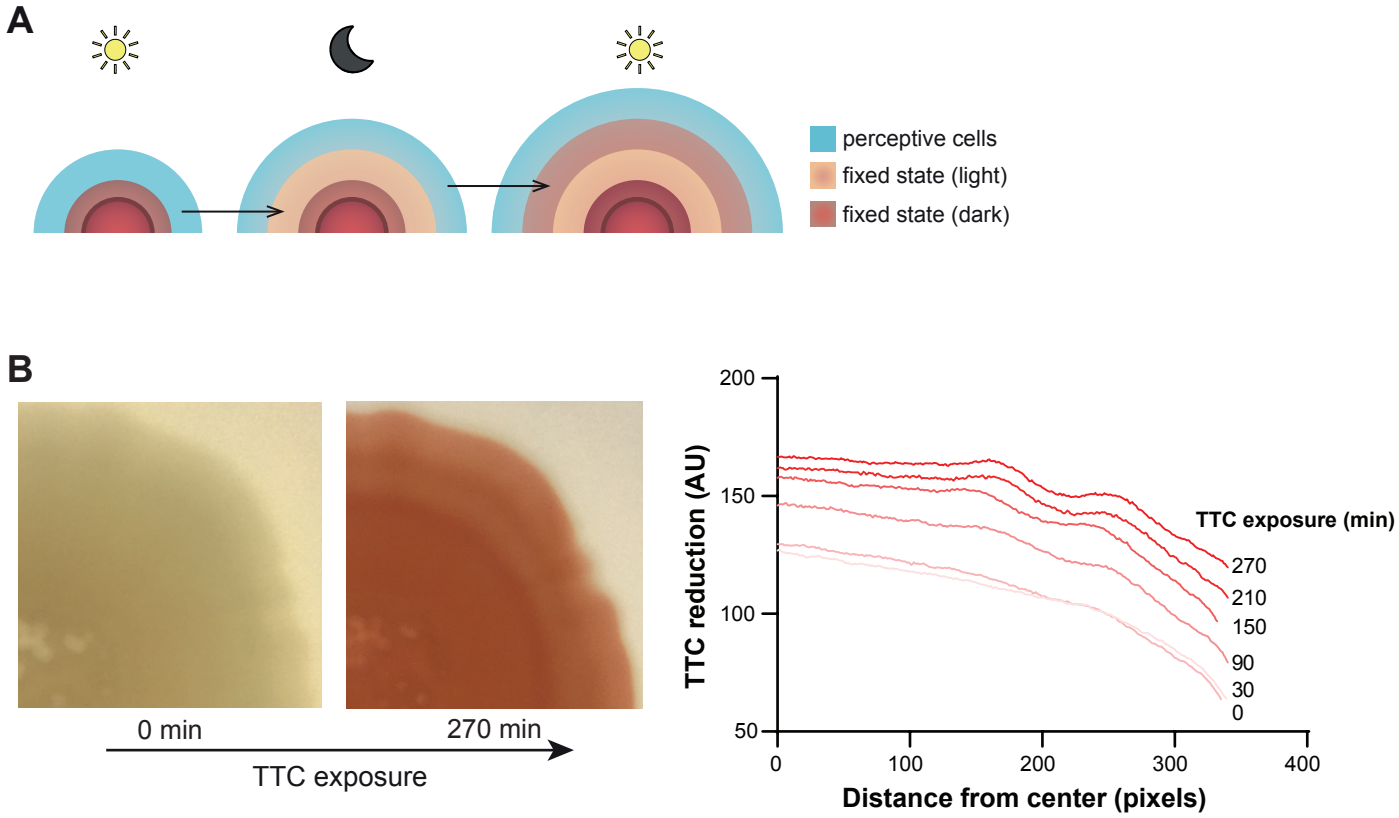

Figure 4. Fixed physiological states are maintained after growth in cycling conditions. (A) Model of biofilm development under cycling conditions: The environmental condition (e.g., light or dark) experienced by perceptive cells at the leading edge of the biofilm (blue) "sets" their physiological status, which then remains fixed through subsequent changes in conditions. **(B)** Left panels: Biofilm coloration after 144 hours of growth under light/dark and 25˚C/23˚C cycling conditions on medium without TTC ("0 min"), and then after transfer to medium containing 0.005% TTC and incubation under constant dark and 23˚C conditions for 270 min. Right panel: Quantification of pixel intensity across a selected radius, at the indicated time points, for the biofilm shown at left.

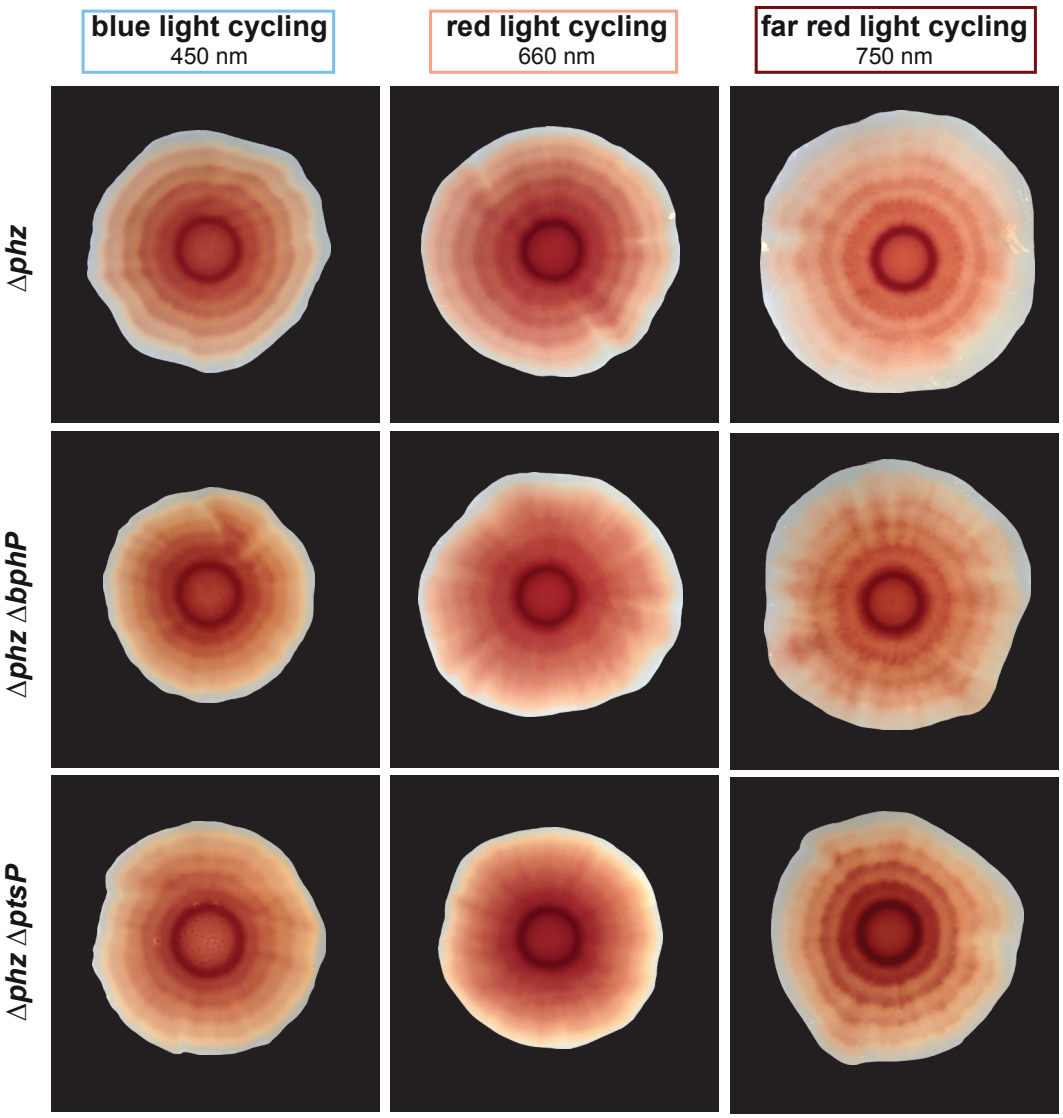

Figure 5. Biofilms grown under light/dark cycling conditions form TTC reduction patterns in blue, red, or far-red light, and Δ*bphP* and Δ*ptsP* mutants show defects in TTC ring pattern formation specifically under red light. TTC reduction patterns in biofilms of the parent strain (Δ*phz*) and indicated mutants grown under light/dark cycling of blue, red, or far-red light with 12-hour intervals. Temperature was kept constant at 25˚C and the growth medium contained 0.004% TTC. Experiments were performed with biological triplicates and representative data are shown.

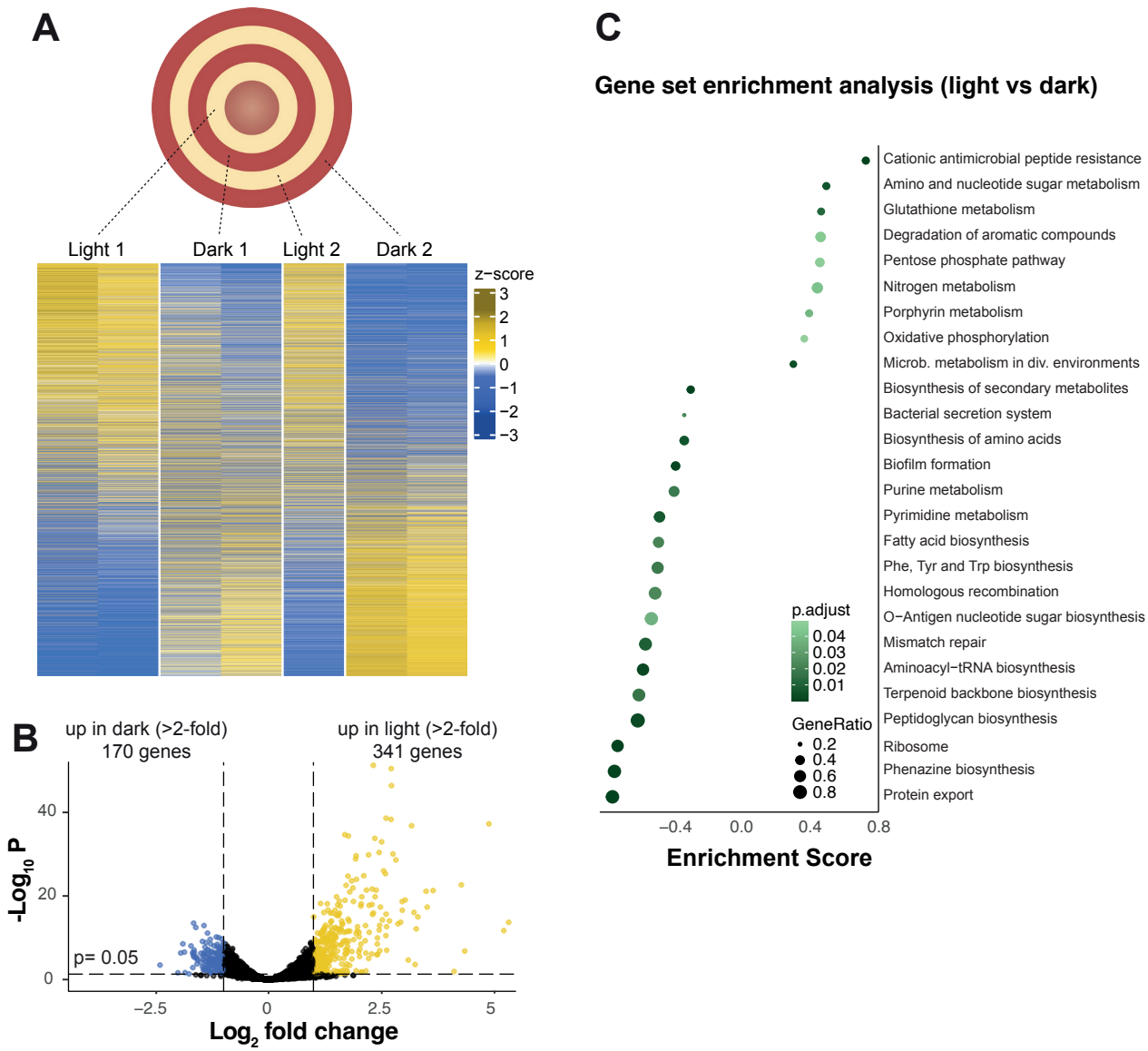

Figure 6. Fixed physiological responses in biofilms grown with light/dark and temperature cycling are evident in differences in transcription. (A) Top: Schematic showing sampling sites in a biofilm grown under cycling conditions on medium containing TTC. The indicated biofilm zones were sampled from duplicate biofilms and subjected to RNAseq. Bottom: Heatmaps representing relative transcript levels (z-scores), shown for each replicate biofilm sample in order of fold change. One sample was omitted because it was determined to be an outlier by principal component analysis. **(B)** Volcano plot showing $\log_2$-transformed average fold change versus statistical significance for each gene, based on normalized transcript levels detected by RNAseq in biofilm zones formed during light vs. dark intervals. Genes that showed a >2-fold increase in expression under dark/23˚C or light/25˚C conditions are represented in blue or yellow, respectively. A total of 5945 genes are represented. **(C)** Gene set enrichment analysis using groups of genes based on KEGG-annotated metabolic pathways. Significant enrichment scores above 0 correspond to over-represented groups of genes in biofilm zones from light intervals, while significant enrichment scores below 0 correspond to over-represented groups of genes in biofilm zones from dark intervals. Gene ratio corresponds to the fraction of genes per pathway contributing to the enrichment.

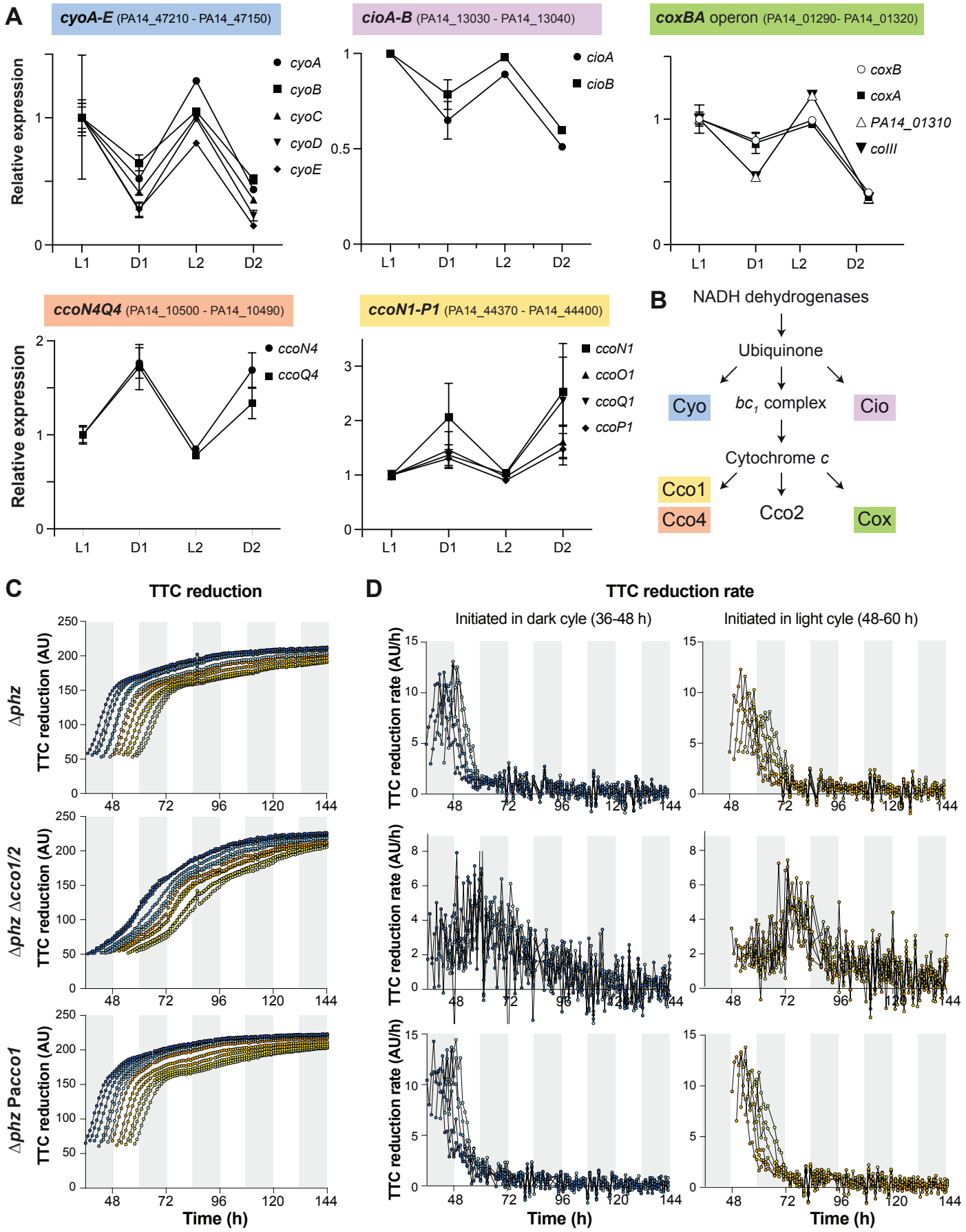
A
cyoA-E (PA14_47210 - PA14_47150)
cyoA
cyoB
cyoC
cyoD
cyoE
Relative expression
L1
D1
L2
D2
cioA-B (PA14_13030 - PA14_13040)
cioA
cioB
coxBA operon (PA14_01290- PA14_01320)
coxB
coxA
PA14_01310
coIII
ccoN4Q4 (PA14_10500 - PA14_10490)
ccoN4
ccoQ4
ccoN1-P1 (PA14_44370 - PA14_44400)
ccoN1
ccoO1
ccoQ1
ccoP1
B
NADH dehydrogenases
Ubiquinone
Cyo
bc1 complex
Cio
Cytochrome c
Cco1
Cco4
Cco2
Cox
C
TTC reduction
TTC reduction (AU)
Δphz
Δphz Δcco1/2
Δphz Pacco1
Time (h)
D
TTC reduction rate
Initiated in dark cyle (36-48 h)
Initiated in light cyle (48-60 h)
TTC reduction rate (AU/h)
Time (h)

Figure 7. Light/dark and temperature cycling affects the expression of PA14 terminal oxidase genes and *cbb*$_3$-type oxidases influence the dynamics of biofilm TTC reduction under this condition. (A) Average relative expression of representative genes that code for subunits of terminal oxidase complexes (source: RNAseq analysis in **Figure 6**). “L1” refers to the “Light 1” ring depicted in Figure 6A (Top), “D1” refers to the “Dark 1” ring, and so on. Error bars indicate the standard deviation of duplicate samples. **(B)** Schematic of *P. aeruginosa*’s branched ETC. Cyo, Cio, Cox, Cco2, and Cco1 are terminal oxidase complexes and Cco4 refers to two “orphan” terminal oxidase subunits that can replace the corresponding subunits in Cco2 or Cco1 (17, 41). **(C)** Pixel intensity over time for selected pixels in biofilms of the indicated strains grown under light/dark and temperature cycling on medium containing 0.004% TTC. **(D)** TTC reduction rate over time for data shown in (C), with data for biomass that formed under dark conditions at left and data for biomass that formed under light conditions at right. For (C) and (D), Data points for biomass formed under dark conditions are blue and those for biomass formed under light conditions are yellow. Darker shades of blue and yellow are used for biomass that formed at earlier time points within an interval and lighter shades are used for biomass that formed at later time points. Results are representative of 3 biological replicates.